

Dark solitons and vortices in \mathcal{PT} -symmetric nonlinear media: from spontaneous symmetry breaking to nonlinear \mathcal{PT} phase transitions

V. Achilleos,¹ P.G. Kevrekidis,² D.J. Frantzeskakis,¹ and R. Carretero-González³

¹Department of Physics, University of Athens, Panepistimiopolis, Zografos, Athens 157 84, Greece

²Department of Mathematics and Statistics, University of Massachusetts, Amherst, Massachusetts 01003-4515, USA

³Nonlinear Dynamical Systems Group, Computational Sciences Research Center,

and Department of Mathematics and Statistics, San Diego State University, San Diego, CA 92182-7720, USA

We consider the nonlinear analogues of Parity-Time (\mathcal{PT}) symmetric linear systems exhibiting defocusing nonlinearities. We study the ground state and excited states (dark solitons and vortices) of the system and report the following remarkable features. For relatively weak values of the parameter ε controlling the strength of the \mathcal{PT} -symmetric potential, excited states undergo (analytically tractable) spontaneous symmetry breaking; as ε is further increased, the ground state and first excited state, as well as branches of higher multi-soliton (multi-vortex) states, collide in pairs and disappear in blue-sky bifurcations, in a way which is strongly reminiscent of the linear \mathcal{PT} -phase transition —thus termed the nonlinear \mathcal{PT} -phase transition. Past this critical point, initialization of, e.g., the former ground state leads to spontaneously emerging “soliton (vortex) sprinklers”.

Introduction. Over the past decade, and since its original inception [1, 2], the theme of \mathcal{PT} -symmetric Hamiltonians has gained considerable momentum in the physics and applied mathematics communities. Such systems, respecting both Parity (\mathcal{P}) and Time-reversal (\mathcal{T}) symmetries —still exhibiting real spectra while non-Hermitian— provided an intriguing alternative to standard Hermitian quantum mechanics. Note that for a standard Schrödinger type Hamiltonian with a generally complex potential U , the \mathcal{PT} symmetry dictates that the potential satisfies the condition $U(x) = U^*(-x)$ [where $(\cdot)^*$ stands for complex conjugation].

Despite the theoretical appeal of such models, it was only recently shown [3] that optics could be an ideal playground for the physical/experimental realization of systems featuring the \mathcal{PT} symmetry. However, this also added another element in the interplay, namely nonlinearity. In that context, the considerations of Ref. [3] extended from bright and gap solitons to linear (Floquet-Bloch) eigenmodes in periodic potentials, examining how these coherent structures are affected by the genuinely complex, yet \mathcal{PT} -symmetric potentials. More recently, experimental results were reported both in nonlinear optical systems [4, 5] and electronic analogs thereof [6]. These, in turn, have triggered a wide range of theoretical studies on nonlinear lattices with either linear [7–15] or nonlinear [16–18] \mathcal{PT} -symmetric potentials and, more recently, on harmonic \mathcal{PT} -symmetric potentials [19].

While the above volume of work has examined numerous features extending from bright solitons to defect modes, and from gap solitons to \mathcal{PT} -lattices, the consideration of defocusing nonlinearities, and especially of dark solitons has been extremely limited (see, e.g., Refs. [20]). Little attention (and again chiefly in the focusing nonlinearity case [3]) has also been paid to \mathcal{PT} -symmetric systems in higher dimensional settings and the corresponding interplay with nonlinear states such as vortices. In the present work, we study systems with \mathcal{PT} -symmetric Hamiltonians exhibiting defocusing nonlinearities, and focus on the existence, stability and dynamical properties of the ground state and excited states, i.e., dark solitons and vortices. Our main findings for a prototypical \mathcal{PT} -symmetric potential, which is harmonic in its real part and

has a localized imaginary part (parametrized by an amplitude parameter ε) are summarized as follows: 1) dark solitons are shown to be subject to spontaneous symmetry-breaking (SSB) instabilities for small ε ; 2) for higher values of ε , the ground state and the first excited state (single dark soliton), as well as pairwise —e.g., 2nd and 3rd, 4th and 5th etc.— higher excited states (respective multiple dark soliton states) are subject to a nonlinear analogue of the \mathcal{PT} -phase transition, colliding and disappearing in a set of blue-sky bifurcations; 3) beyond this critical point, the system acts as a soliton sprinkler, spontaneously emitting dark multi-soliton structures. 4) All of these features have direct counterparts for vortices in two-dimensional settings, illustrating the generic nature of these findings.

Fundamental States: Ground State and Dark Soliton. Our model, motivated by the above nonlinear optical considerations (but also by ones pertinent to nonlinear phenomena in Bose-Einstein condensates (BECs) [21]), will be, for the one-dimensional (1D) setting, as follows:

$$i\partial_t u = -\frac{1}{2}\partial_x^2 u + |u|^2 u + [V(x) + iW(x)]u, \quad (1)$$

where u is the complex electric field envelope (or the macroscopic wavefunction in BECs), t denotes the propagation distance (or time in BECs) and x is the transverse direction. For a \mathcal{PT} -symmetric Hamiltonian, the real and imaginary parts of the potential must satisfy $V(x) = V(-x)$ and $W(x) = -W(-x)$. Below we focus on the case of a real parabolic potential, $V(x) = (1/2)\Omega^2 x^2$, modeling the transverse distribution of the refractive index (or the external trap in BECs), while the imaginary part $W(x)$ is considered to be an odd, localized function of spatial width $\ll \Omega^{-1}$. A generalization of this model will be studied below in two-dimensions (2D), with $V = (1/2)\Omega^2(x^2 + y^2)$ and $W = \varepsilon(x + y)e^{-(x^2 + y^2)/4}$.

We now analyze the fundamental states (namely the ground state and the first excited —single dark soliton— state of the system) shown in Fig. 1. We seek stationary solutions of Eq. (1) in the form $u = u_b(x) \exp(-i\mu t)$, where μ is the propagation constant (or the chemical potential in BECs). For a sufficiently small imaginary potential, $W(x) = \varepsilon \tilde{W}(x)$ [with

$\max\{|\tilde{W}(x)|\} = O(1)$, where $\varepsilon \ll 1$, and when the inverse width Ω^{-1} of $V(x)$ is sufficiently large, $\Omega \sim \varepsilon$, we may find—in the Thomas-Fermi (TF) limit—an approximate solution of Eq. (1). This is of the form $u_b = [\sqrt{\mu} + f(x)] \exp[i\phi(x)]$, where the amplitude and phase $f(x)$ and $\phi(x)$ (considered to be small, of order ε^2 and ε , respectively) are given by:

$$f(x) = -\frac{1}{2\sqrt{\mu}} (V + 2W^2), \quad \phi(x) = 2 \int W dx. \quad (2)$$

where $W = \int W dx$. Contrary to the conservative case ($\varepsilon = 0$) [21], this TF background is characterized by a density dip located at the center ($x = 0$) and a nontrivial phase distribution. Both features are shown in the top panels of Fig. 1, where the analytical result is compared with the numerical. Importantly, a linear stability—Bogoliubov-de Gennes (BdG)—analysis (see, e.g., Ref. [25]) shows that the background $u_b(x)$ is stable against small perturbations. Here we notice that the evolution of the power, $N = \int |u|^2 dx$, is governed by the equation $dN/dt = 2 \int |u_b|^2 W(x) dx$ and, thus, for u_b even and $W(x)$ odd, it is conserved. This conservation also holds for excited states sharing the parity of $|u_b|^2$.

To describe the dynamics of a dark soliton (DS) $v(x, t)$ on top of this TF background, we introduce the ansatz $u = u_b(x)v(x, t)$ into Eq. (1) and, after using the scale transformations $t \rightarrow \mu t$ and $x \rightarrow \sqrt{\mu}x$, we obtain the following perturbed nonlinear Schrödinger (NLS) equation:

$$i\partial_t v + \frac{1}{2}\partial_{xx}v + v(1 - |v|^2) = \mu^{-2}P(v), \quad (3)$$

where the perturbation [which is of order $O(\varepsilon^2)$] is given by

$$P(v) = (1 - |v|^2)v(V + 2W^2) + v_x \left(\frac{1}{2}V_x - 2(W - i)W \right).$$

Applying the perturbation theory for dark solitons [25], we seek a solution of Eq. (3) in the form of the dark soliton of the unperturbed system ($P(v) = 0$): $v(x, t) = \cos \varphi(t) \tanh \xi + i \sin \varphi(t)$, where $\xi \equiv \cos \varphi(t) [x - x_0(t)]$, with $\varphi(t)$ and $x_0(t)$ being the slowly-varying phase and center of the soliton. In the adiabatic approximation $dx_0/dt = \sin \varphi$, while the perturbation-induced evolution equation for φ reads:

$$\frac{d\varphi}{dt} = -\frac{1}{2}\partial_x V - \int \text{sech}^4(\xi) [\tanh(\xi)W^2 + WW] dx, \quad (4)$$

where we have assumed almost black solitons with $\cos \varphi \approx 1$. This way, for a given $W(x)$, we can derive an equation of motion for the soliton center x_0 . Hereafter, we consider an imaginary potential of the form $W(x) = \varepsilon x \exp(-x^2/2)$ (other choices, e.g., $W = \varepsilon \text{sech}^2(x) \tanh(x)$ have led to similar results). To examine the stability of the equilibrium at $x_0 = 0$, we Taylor expand Eq. (4), obtaining to leading order

$$\frac{d^2 x_0}{dt^2} = -\omega_{\text{osc}}^2 x_0, \quad \omega_{\text{osc}}^2 \approx \left(\frac{\Omega}{\sqrt{2}} \right)^2 - \frac{6}{5}\varepsilon^2. \quad (5)$$

Equation (5) implies that if the amplitude ε of $W(x)$ is less than a critical value $\varepsilon_{cr}^{(1)} = \sqrt{5/12}\Omega$, the soliton performs

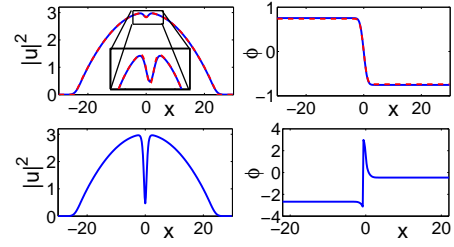


FIG. 1: (Color online) Fundamental states. Top: Density (left) and phase (right) of the numerically obtained TF background [solid (blue) line] compared to the prediction of Eqs. (2) [dashed (red) line]; the inset shows the characteristic density dip induced by $W(x)$ at the origin. Bottom: The same properties are shown now for the (single) dark soliton. Parameters values are: $\mu = 3$, $\Omega = 0.1$ and $\varepsilon = 0.3$.

oscillations in the complex potential with frequency ω_{osc} ; on the other hand, if $\varepsilon > \varepsilon_{cr}^{(1)}$ the soliton becomes unstable. The above prediction has been confirmed numerically, both by means of direct simulations and employing a BdG analysis. The latter reveals that the considered stationary dark soliton is characterized by the anomalous mode eigenfrequency ω_α [24, 25], which is real for $\varepsilon < \varepsilon_{cr}^{(1)}$ (in this case, $\omega_\alpha = \omega_{\text{osc}}$), and it becomes imaginary for $\varepsilon > \varepsilon_{cr}^{(1)}$, thus signaling the onset of the SSB instability of the dark soliton (which displaces the soliton from the trap center).

The dependence of ω_α^2 on the amplitude ε of the imaginary potential W , as found by the BdG analysis, is illustrated in the top panel of Fig. 2. As shown in the inset, ω_α^2 initially moves towards the spectral plane origin, and past the critical point, $\varepsilon_{cr}^{(1)}$ (cf. vertical line), ω_α exits as an imaginary pair of eigenfrequencies manifesting the soliton's exponential instability. As shown in the top panel, for small ε , the agreement between the analytical prediction of Eq. (5) [(red) line] and the BdG numerical result [(blue) circles] is excellent.

From symmetry breaking to nonlinear \mathcal{PT} transitions. For larger values of ε , the unstable imaginary eigenvalue, makes a maximal excursion along the imaginary line and returns to the origin at a second critical point, $\varepsilon_{cr}^{(2)} = 0.62$, finally colliding with it. The branch of single soliton solutions disappears past this critical point. To better understand how the branch ceases to exist, we first observe (bottom panel of Fig. 1) that the density profile of the soliton becomes increasingly shallower (i.e., more “grey”) as ε grows and the second critical point is approached. This is due to the development of an increasingly strong *even* imaginary part of the solution. Furthermore, the stable background (ground state) solution $u_b(x)$ [cf. Eqs. (2) and top panel of Fig. 1] develops an *odd* imaginary part resembling a (progressively darker) grey soliton. Finally, at $\varepsilon = \varepsilon_{cr}^{(2)}$, the profiles of these modes become identical and disappear in a blue-sky bifurcation through their collision. This is shown in the bottom panel of Fig. 2, where the power N is shown as a function of ε . The top solid (blue) branch shows the stable ground state, u_b , which ultimately collides with the one soliton (first excited) state at $\varepsilon \approx 0.62$ (for $\mu = 3$ and $\Omega = 0.1$).

Importantly, we have confirmed that the above description

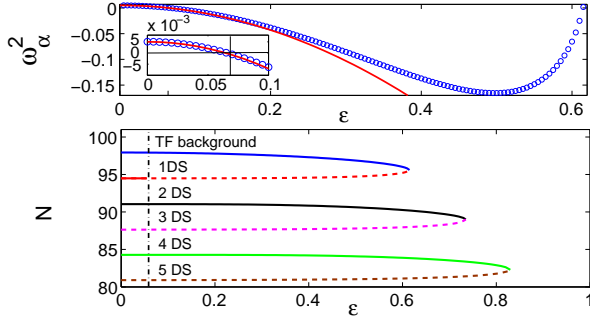


FIG. 2: (Color online) Bifurcations/instabilities of nonlinear states. Top panel: the dependence of the soliton’s squared eigenfrequency, ω_α^2 , on the amplitude ε of $W(x)$; the inset shows a detail near the critical value $\varepsilon_{cr}^{(1)}$ (vertical line), where it crosses the origin. The (blue) circles and the (red) line depict, respectively, numerical (BdG) and analytical [cf. Eq. (5)] results. Bottom panel: the full bifurcation diagram (denoting the above instability by a vertical line and) encompassing the pairwise bifurcations/disappearances of the nonlinear states. Solid (dashed) lines indicate dynamically stable (unstable) branches. Here, $\mu = 3$ and $\Omega = 0.1$.

holds also for higher excited states (multiple dark soliton solutions), as shown in Fig. 2: each pair of the higher excited states (2nd with 3rd, 4th with 5th etc.) also disappears in a blue-sky bifurcation. A general remark is that higher excited states bifurcate for larger values of ε . Remarkably, this can be thought of as a *nonlinear analogue* of the \mathcal{PT} transition, in analogy with the pairwise collisions in Ref. [1] (see e.g. Fig. 1 of that reference) for the linear setting [26].

A relevant question concerns the dynamics of the nonlinear waves when subject to these (SSB and blue-sky) bifurcations. To answer this, we numerically integrated Eq. (1) as shown in Fig. 3. In the top panels, we have illustrated the dynamics of the DS upon its destabilization at $\varepsilon = \varepsilon_{cr}^{(1)}$. When the SSB is manifested, the soliton is either spontaneously ejected towards the lossy side (and typically found to localize therein while the background grows in amplitude and widens) or moves to the gain side executing oscillations thereafter. On the other hand, past $\varepsilon = \varepsilon_{cr}^{(2)}$, using, as an initial condition the form of the TF background (bottom panel of Fig. 3), we have found that a dark soliton train is spontaneously formed, with an increasingly larger number of solitons as larger values of ε are used (i.e., a “soliton sprinkler” emerges). This can be intuitively connected to the observation of Fig. 2 that higher excited multi-soliton states persist for larger ε than lower ones. Again, it is typically observed that the solitons are nucleated and stay in the vicinity of the global minimum of $W(x)$, which indicates the “lossy” side of the imaginary potential.

Two-dimensional Generalizations. The bifurcation of the nonlinear structures emerging in 2D follows a similar, but also more complex, pattern than in the corresponding 1D setting. Figure 4 depicts the full bifurcation scenario for solutions bearing no vortices (the TF background cloud), one to six vortices, and the dark soliton stripe. As in 1D, the TF background is stable in all its domain of existence and collides, in a blue-sky bifurcation, for a large enough value of ε , with an excited

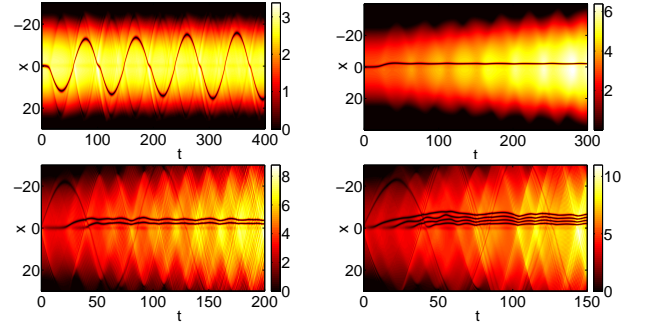


FIG. 3: (Color online) Bifurcation-induced dynamics. Top panels: manifestations of the SSB destabilization scenarios for an unstable dark soliton past $\varepsilon = \varepsilon_{cr}^{(1)}$. Bottom panels: soliton sprinkler spontaneously leading to two or four solitons from the ground state used for $\varepsilon > \varepsilon_{cr}^{(2)}$. The parameters are $\mu = 3$ and $\Omega = 0.1$ and $\varepsilon = 0.3$ (top row), $\varepsilon = 0.64$ (bottom left), and $\varepsilon = 0.7$ (bottom right).

state. However, in contrast to the 1D case where this collision happens with the first excited state, in 2D the collision occurs with the *second* excited state, due to the absence of net topological charge in such a vortex-dipole (see top-right red curve) bearing two opposite charge vortices emerging from the central dip of the TF background. At this critical point $\varepsilon = \varepsilon_{cr}^{(2)}$ the dipole branch is unstable, having been destabilized through an SSB bifurcation at an $\varepsilon = \varepsilon_{cr}^{(1)} > 0$ value (below which for $\varepsilon > 0$ the dipole is stable —see portion of red solid line in the figure). As this branch is followed (from top to bottom in the figure) a series of bifurcations occur where the existing vortices are drawn to the periphery of the cloud, a dip in the center deepens leading eventually to a new vortex pair emerging (i.e., a higher excited state). In this manner the branches with *even* number of vortices are all connected. As more and more vortex pairs emerge, the cloud “saturates” and can no longer fit in new vortex pairs finally colliding with a dark soliton stripe (see lower blue branch in the figure). This overall bifurcation structure of even vortex numbers—with a $\varepsilon \rightarrow -\varepsilon$ symmetry where the solutions are just flipped by $(x, y) \rightarrow (-x, -y)$ —is depicted, with density and phase profiles, in the series of panels of Fig. 4(b).

As for the bifurcation scenario of *odd* number of vortices, the first excited state bearing a single vortex at the origin (for $\varepsilon = 0$) is stable for small values of ε , while it again sustains an SSB bifurcation for larger ε . As ε increases the vortex moves towards the periphery of the cloud and a dip at the center of the cloud deepens until a vortex pair emerges from it. This scenario connects the one-vortex branch with the *asymmetric* three-vortex (+ − + vortex tripole) branch, as it is depicted with the top (magenta and green) lines in panel 4(a) and the series of snapshots in panels 4(c). As it is evident from the figure, the asymmetric three-vortex branch eventually connects with the symmetric one for values of $\varepsilon \rightarrow 0$. A similar bifurcation occurs with the symmetric three-vortex branch, which becomes asymmetric with a deepening dip at the center where a vortex pair emerges (at the same time that a vortex is lost at the periphery), connecting in this way with the four-vortex branch [see series of snapshots in panels 4(d)].

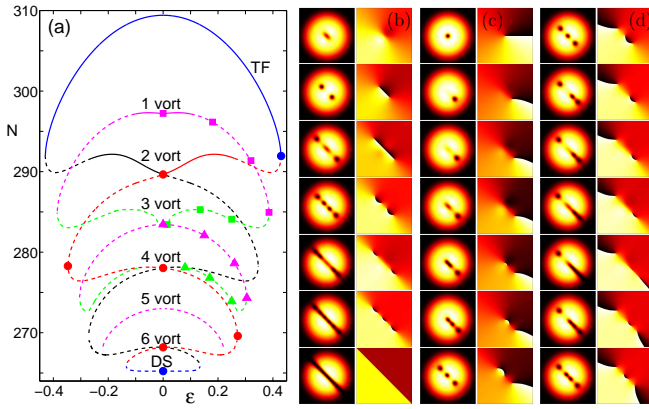


FIG. 4: (Color online) The 2D generalization. (a) Bifurcation diagram for the 2D stationary nonlinear (vortex and DS stripe) states. Stable (unstable) branches, as per the corresponding BdG analysis, are depicted with solid (dashed) lines. (b) Series of density (left) and phase (right) configurations along the branch with even number of vortices corresponding to the circles in panel (a) [from top to bottom]. (c) Same as (b) for the branch starting with one vortex and connecting with three vortices corresponding to the squares in panel (a) [from top to bottom]. (d) Same as (b) for the branch starting with three symmetric vortices and ending with four vortices corresponding to the triangles in panel (a) [from top to bottom]. Parameter values are: $\mu = 2$ and $\Omega = 0.2$. The field of view for the configurations is $[-10.5, 10.5] \times [-10.5, 10.5]$.

As for the dynamics of unstable steady states, we have observed—in analogy with the 1D case—that (a) a single vortex tends to migrate towards the minimum of the lossy side of the potential, while the remaining vortices (if present) perform almost circular orbits at the periphery of the cloud where they are eventually absorbed; and (b) past $\varepsilon = \varepsilon_{cr}^{(2)}$, using as an initial condition the form of the TF background, also produces

the spontaneous formation of an increasing number of vortices for larger values of ε (namely, a “vortex sprinkler”). It is worth mentioning that the precise structure of the bifurcation diagram depends of the values of the propagation constant μ and the trap strength Ω . For weaker Ω and/or larger μ the extent of the TF background will be larger allowing for a longer bifurcating chain of higher-order vortex states. Nonetheless, the displayed SSB instabilities and phenomenology and the nonlinear \mathcal{PT} transition involving the cascade of blue-sky bifurcations (notice that in the 2D case the order is reversed and the largest ε bifurcation is that involving the TF and the dipole states) appear to be universal in confining \mathcal{PT} -symmetric potentials.

Conclusions. In the present work, we have developed some fundamental insights stemming from the interplay of defocusing nonlinearity and \mathcal{PT} -symmetric confining potentials. We identified both a symmetry-breaking bifurcation destabilizing the dark solitons that leads to non-stationary dynamics, as well as a nonlinear analogue of the \mathcal{PT} transition that eventually terminates both the ground state and the dark soliton branch, yielding purely gain-loss dynamics within the system. Similar bifurcation phenomena and dynamics of mobility or of spontaneous emergence of dynamical patterns forming out of the destabilization of the nonlinear states were identified in two-dimensional settings, for vortices. These investigations, we believe, pave the way for studying \mathcal{PT} -symmetric systems in the context of defocusing nonlinearities and of higher dimensional systems, which are some of the natural extensions of the \mathcal{PT} -symmetric literature. A canonical set of investigations which is still missing concerns the effects of such potentials in three-dimensional continuum or higher dimensional lattice contexts, as well as the manipulation of nonlinear states emerging in these systems. These will be pursued in future works.

-
- [1] C.M. Bender and S. Boettcher, Phys. Rev. Lett. **80**, 5243 (1998).
 - [2] C.M. Bender, S. Boettcher, and P.N. Meisinger, J. Math. Phys. **40**, 2201 (1999); C.M. Bender, Rep. Prog. Phys. **70**, 947 (2007).
 - [3] Z. H. Musslimani, K. G. Makris, R. El-Ganainy, and D. N. Christodoulides, Phys. Rev. Lett. **100**, 030402 (2008); K.G. Makris, R. El-Ganainy, D.N. Christodoulides and Z.H. Musslimani, Phys. Rev. A **81**, 063807 (2010).
 - [4] A. Guo, G. J. Salamo, D. Duchesne, R. Morandotti, M. Volatier-Ravat, V. Aimez, G. A. Siviloglou and D. N. Christodoulides, Phys. Rev. Lett. **103**, 093902 (2009).
 - [5] C.E. Rüter, K.G. Makris, R. El-Ganainy, D.N. Christodoulides, M. Segev, D. Kip, Nature Phys. **6**, 192 (2010).
 - [6] J. Schindler, A. Li, M.C. Zheng, F.M. Ellis and T. Kottos, Phys. Rev. A **84**, 040101 (2011).
 - [7] H. Ramezani, T. Kottos, R. El-Ganainy and D.N. Christodoulides, Phys. Rev. A **82**, 043803 (2010).
 - [8] A.A. Sukhorukov, Z. Xu and Yu.S. Kivshar, Phys. Rev. A **82**, 043818 (2010).
 - [9] M.C. Zheng, D.N. Christodoulides, R. Fleischmann and T. Kottos, Phys. Rev. A **82**, 010103(R) (2010).
 - [10] E.M. Graefe, H.J. Korsch and A.E. Niederle, Phys. Rev. Lett. **101**, 150408 (2008).
 - [11] E.M. Graefe, H.J. Korsch and A.E. Niederle, Phys. Rev. A **82**, 013629 (2010).
 - [12] Z. Lin, H. Ramezani, T. Eichelkraut, T. Kottos, H. Cao and D.N. Christodoulides, Phys. Rev. Lett. **106**, 213901 (2011).
 - [13] K. Li and P. G. Kevrekidis, Phys. Rev. E **83**, 066608 (2011).
 - [14] S. V. Dmitriev, S. V. Suchkov, A. A. Sukhorukov, and Yu. S. Kivshar, Phys. Rev. A **84**, 013833 (2011).
 - [15] S. V. Suchkov, B. A. Malomed, S. V. Dmitriev and Yu. S. Kivshar, Phys. Rev. E **84**, 046609 (2011).
 - [16] A.E. Miroshnichenko, B.A. Malomed, and Yu.S. Kivshar Phys. Rev. A **84**, 012123 (2011).
 - [17] F. Kh. Abdullaev, Y. V. Kartashov, V. V. Konotop and D. A. Zezyulin, Phys. Rev. A **83**, 041805 (2011).
 - [18] D. A. Zezyulin, Y. V. Kartashov, V. V. Konotop, Europhys. Lett. **96**, 64003 (2011).
 - [19] D. A. Zezyulin and V. V. Konotop, arXiv:1201.6638.
 - [20] H. G. Li, Z. W. Shi, X. J. Jiang, and X. Zhu, Opt. Lett. **36**, 3290 (2011).
 - [21] P. G. Kevrekidis, D. J. Frantzeskakis, and R. Carretero-González, *Emergent Nonlinear Phenomena in Bose-Einstein*

- Condensates: Theory and Experiment* (Springer-Verlag, Heidelberg, 2008).
- [22] S. Flach, Y. Zolotaryuk, and K. Kladko Phys. Rev. E **59**, 6105 (1999).
 - [23] Kh. I. Pushkarov, D. I. Pushkarov, I. V. Tomov, Opt. Quant. Electr. **11**, 471 (1979); Kh. I. Pushkarov, D.I. Pushkarov, Rep. Math. Phys. **17**, 37 (1980); S. Cowan, R. H. Enns, S. S. Rangnekar, S. S. Sanghera, Can. J. Phys. **64**, 311 (1986); J. Herrmann, Opt. Commun. **87**, 161 (1992).
 - [24] G. Theocharis, P. G. Kevrekidis, M. K. Oberthaler, and D. J. Frantzeskakis Phys. Rev. A **76**, 045601 (2007); G. Theocharis, A. Weller, J. P. Ronzheimer, C. Gross, M. K. Oberthaler, P. G. Kevrekidis, and D. J. Frantzeskakis Phys. Rev. A **81**, 063604 (2010).
 - [25] D. J. Frantzeskakis, J. Phys. A: Math. Theor. **43**, 213001 (2010).
 - [26] Despite the similarity of the two figures, it does not escape us that an interesting difference exists: in the linear picture the lowest eigenvalues collide the last, while in the 1D nonlinear case the lowest eigenstates disappear the first, a feature that important consequences for the supercritical dynamics of Fig. 3.